Key Points:
- Citizen scientists discover a new auroral form, named the dunes, presenting a large-scale monochromatic wave field
- We develop a triangulation method using citizen scientist photographs as science data
- We suggest that the dunes manifest mesospheric bores, which have not previously been observed in the diffuse aurora

Supporting Information:
- Supporting Information S1
- Original Version of Manuscript
- Peer Review History
- First Revision of Manuscript [Accepted]

Correspondence

M. Palmroth,
minna.palmroth@helsinki.fi

Citizen Scientists Discover a New Auroral Form: Dunes Provide Insight Into the Upper Atmosphere

M. Palmroth[1,2], M. Grandin[1], M. Helin[3], P. Koski[3], A. Oksanen[4], M. A. Glad[3], R. Valonen[3], K. Saari[3], E. Bruus[5], J. Norberg[2], A. Viljanen[2], K. Kauristie[2], and P. T. Verronen[2,6]

[1]Department of Physics, University of Helsinki, Helsinki, Finland, [2]Space and Earth Observation Centre, Finnish Meteorological Institute, Helsinki, Finland, [3]Citizen Scientist, Finland, [4]Hankasalmi Observatory, Jyväskylän Sirius ry, Hankasalmi, Finland, [5]Taivaanvahti Service, Finnish Association of Amateur Astronomers (Ursa), Helsinki, Finland, [6]Sodankylä Geophysical Observatory, University of Oulu, Oulu, Finland

Abstract Auroral forms are like fingerprints linking optical features to physical phenomena in the near-Earth space. While discovering new forms is rare, recently, scientists reported of citizens' observations of STEVE, a pinkish optical manifestation of subauroral ionospheric drifts that were not thought to be visible to the naked eye. Here, we present a new auroral form named "the dunes". On 7 October 2018, citizen observers took multiple digital photographs of the same dunes simultaneously from different locations in Finland and Sweden. We develop a triangulation method to analyze the photographs and conclude that the dunes are a monochromatic wave field with a wavelength of about 45 km within a thin layer at 100 km altitude. Supporting data suggest that the dunes manifest atmospheric waves, possibly mesospheric bores, which are rarely detected, and have not previously been observed via diffuse aurora nor at auroral latitudes and altitudes. The dunes present a new opportunity to investigate the coupling of the lower/middle atmosphere to the thermosphere and ionosphere. Our paper adds to the growing body of work that illustrates the value of citizen scientist images in carrying out quantitative analysis of optical phenomena, especially at small scales at subauroral latitudes. Further, the dune project presents means to create general interest toward physics, emphasizing that citizens can take part in scientific work by helping to uncover new phenomena.

Plain Language Summary Above Earth's atmosphere at about 80–120 km altitude, lies a region that is often dubbed as the "ignorosphere," one of the least explored regions at our planet. We present a new auroral form spotted by citizen scientists and show how it can be used to investigate the ignorosphere. We name the new form as "the dunes" and develop a method to analyze the citizen scientist pictures using the stars on the skies as reference points. The new method and other supporting data indicate that the dunes are a monochromatic wave field with a wavelength of about 45 km within a thin layer at 100 km altitude, right in the ignorosphere, where atmosphere meets the electromagnetic forcing from space. The analysis suggests that the dunes manifest atmospheric waves, possibly a rare phenomenon called mesospheric bores, which are large wave fields propagating in the ignorosphere. They have not previously been observed via aurora, nor at auroral latitudes and altitudes. The dunes present a new opportunity to investigate the ignorosphere and its driving from above. Further, the dune project presents means to create general interest toward physics, emphasizing that citizens can take part in scientific work by helping to uncover new phenomena.

1. Introduction

The auroral mesosphere-lower thermosphere-ionosphere (MLTI) region, often dubbed as the "ignorosphere" at about 65–80° in geographic latitude and at 80–120 km altitude is one of the most intriguing regions within the near-Earth space. This is because the conditions at auroral latitudes are controlled by a multitude of drivers making the environment highly variable. The atmospheric conditions are characterized by diurnal and seasonal variability due to changes in the solar heating. In addition, the atmospheric conditions are driven by electromagnetic forcing from ionosphere and magnetosphere (Andersson et al., 2014; Arnold & Robinson, 2001). The high-latitude ionospheric conditions are controlled by the solar wind energy, which is extracted by various processes within the Earth's magnetosphere and deposited into the ionosphere through Joule heating and particle precipitation (Palmroth et al., 2005, 2006). This ionospheric
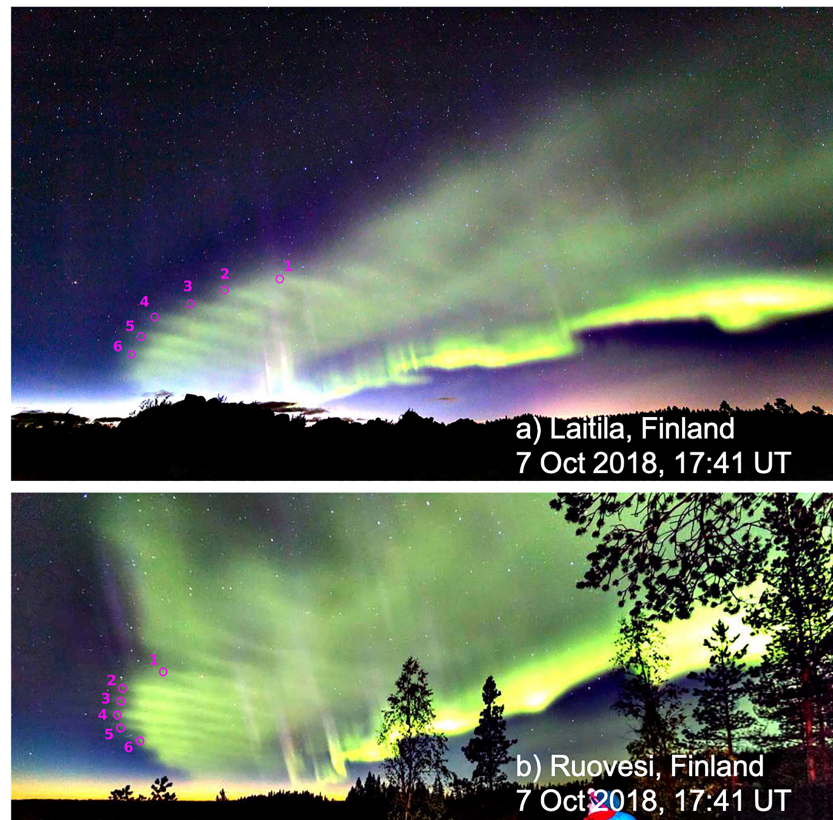
Figure 1. (a) Auroral dunes captured on 7 October 2018, at 17:40.59 UT in Laitila (see location in Figure 4b). The stars in the background indicate that the field of view is toward the northwest. The dunes (marked by magenta circles and numbers, which refer to section 2) extend equatorward from the discrete bright arc in the north. The local magnetic field direction is shown by the auroral pillars, the almost vertical purple structures. (b) Simultaneous picture of the dunes in Ruovesi, 172 km northeast from Laitila. The background star positions indicate that the field of view is roughly toward the west.

energy deposition leads to highly variable plasma flows and conductivity distributions (Lu, 2017) and vivid auroral displays. Further, the neutral atmospheric conditions affect the ionospheric electrodynamics at least through ion chemistry and coupling the neutral winds with the Joule heating process (Aikio et al., 2012; Marchaudon et al., 2018). Hence, the auroral MLTI region is characterized by complex dynamics between the neutral atmosphere and the electromagnetic ionosphere.

The auroral MLTI region is notoriously difficult to measure, hence the term ignorosphere. Spacecraft would need to make significant use of thrust to maintain their orbit due to the large neutral densities, and different ground-based instruments are either not located suitably underneath the phenomena of interest or do not reach the altitudes of interest. For example, the neutral atmospheric waves, which couple to the electrodynamics, are observed using airglow instruments, lidars, and riometers up to about 90 km (Ehard et al., 2014; Jarvis et al., 2003; Smith et al., 2000). Higher than this, one can use radars and optical imagers (Shiokawa et al., 2012; Röttger, 1994) but these are often located at the typical auroral latitudes, excluding subauroral regions. The atmospheric waves are generally not investigated using auroral emission in the previous literature.

Improving digital camera technology has inspired amateur photographers to capture artistic shots featuring aurora and other night-sky optical phenomena. Citizen photographs have led to surprising scientific advances and received worldwide attention. Though technically not an aurora, the Strong Thermal Emission Velocity Enhancement (STEVE) project (Gallardo-Lacourt et al., 2018; MacDonald et al., 2018) has linked subauroral ion drifts (Anderson et al., 1991) to mauve-colored optical features on the night skies. As a result, a growing body of new information has been gathered of the STEVE phenomenon, and it has
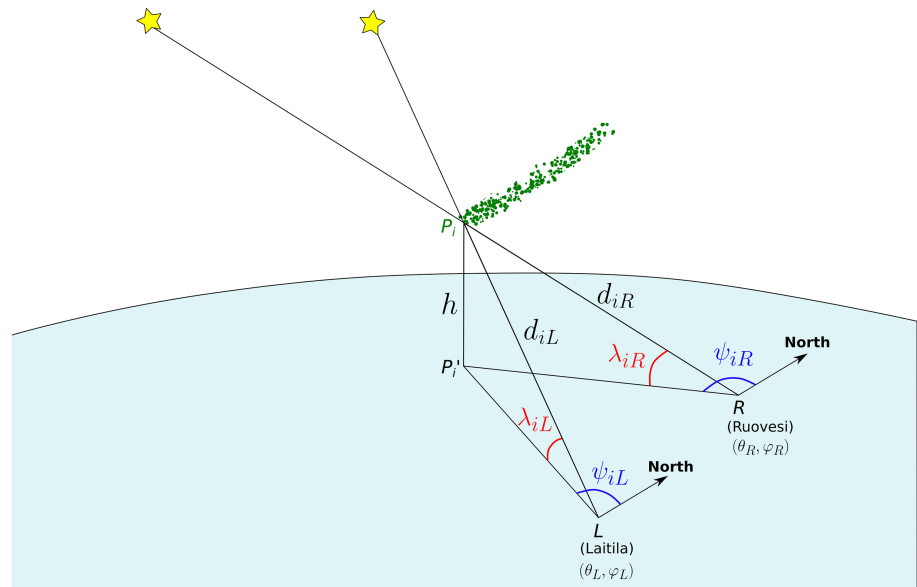
Figure 2. (a) Dunes on 7 October 2018, at 17:34 UT in Siilinjärvi (about 250 km northeast from Ruovesi). The stars in the background indicate that the field of view is toward the west. The photograph includes the same bright arc toward the north, seen in Figure 1. The local magnetic field direction is shown by the auroral pillars. (b) All-sky-camera image from 17:28 UT in Hankasalmi, showing the dunes with a white arrow. Geographic directions (with east and west flipped) are given with a black mark at the edge of the image, and the brightest stars are marked with red.

recently been suggested that the emission could also be associated with ionospheric heating by heat flux, ion-neutral friction, or low-energy precipitation (Nishimura et al., 2019).

Following a popular guidebook project to explain auroral forms to citizen observers (Palmroth et al., 2018), a group of Finnish auroral enthusiasts reported of several events with an unexplained auroral form presenting a monochromatic wave field in the auroral emission. They named the waves as *the dunes*. On 7 October 2018, the auroral watchers spotted the dunes again, this time marking the start of a detective story uncovering the physics the dunes represent. We organized an ad hoc campaign in the evening of 7 October 2018, where the scientists and the citizen observers from different parts of Finland were in real-time connection. As a result, we gained several consecutive and simultaneous pictures with calibrated camera clocks throughout Finland. These pictures, presented in this paper, formed the backbone of this study.

Figure 1a shows a result of the 7 October 2018 campaign, a picture of the aurora on the night sky, with background stars indicating a field of view toward the northwest. Figure 1a shows that the main bright arc

Figure 3. Geometry of the dune mapping procedure using two simultaneous pictures taken from Laitila and Ruovesi (Figure 1), see text for details.

is located in the north, and additionally there are finger-like rays of green emission extending equatorward from the bright arc. These finger-like rays are called the dunes, pictured in Laitila in south-western Finland at 17:41 UT, where they were visible during 17:39–17:59 UT. Figure 1b shows the dunes simultaneously in Ruovesi, 172 km northeast from Laitila. Figure 2a shows the dunes in Siilinjärvi, about 250 km northeast from Ruovesi, taken at 17:34 UT. Figure 2b illustrates how the dunes are presented with an all-sky-camera, featuring the dunes in Hankasalmi at 17:28 UT. The dunes were visible at Siilinjärvi around 17:34–17:58 UT, while most of the Hankasalmi images during the time of dune observations at other locations were covered with clouds. Supporting information Movie S1 shows the dunes in Savojärvi, located about 40 km southeast from Laitila, where they were visible during 17:33–17:51 UT.

This article presents the auroral dunes as a phenomenon and ties them to atmospheric waves. Before we can fully characterize the dunes, we first introduce the method we developed to analyze the digital photographs, in section 2. Section 3 presents other supporting data characterizing the dunes and their environmental conditions. We conclude in section 4 by suggesting that the dunes present a new opportunity to observe the ignorosphere and that they offer a possibility to investigate coupling of the lower/middle atmosphere to the thermosphere and ionosphere.

2. Methods

Using simultaneous pictures it is possible to estimate the altitude of the dunes using the background stars as reference points for trigonometric calculations. This triangulation method is based on identifying same dunes within two simultaneous images, after which the azimuth and elevation of each dune fingertip can be determined by finding which stars can be seen behind them (see Figure 3). The star positions can be accurately determined by using the open source Stellarium software (Chereau, 2019) and by setting the observation time and locations to be exactly those of the two pictures. The established dune altitude can be used as a reference to determine their mapping to the ground to infer the wavelength of the dune field.

2.1. Altitude Determination
The altitude of the dunes was estimated using simultaneous pictures of the same dune field, presented in Figure 1, taken at 17:41 UT from two locations in Finland (Laitila and Ruovesi), which are separated by 172 km. A great property of the night sky is that there is a known star behind each dune fingertip. In each picture, the equatorward tips of six dunes were identified unambiguously thanks to the presence of a shorter dune in the dune field, visible in both Figures 1a and 1b. The six dune fingertips are indicated with numbers 1–6 starting from the shorter dune in the pictures. For each visually identified dune tip, we searched for a corresponding object cataloged in the Stellarium software (Chereau, 2019), which calculates the angular

Table 1
Mapping of the Equatorward Tips of Dunes Observed From Laitila and Ruovesi at 17:41 UT

Dune number		1	2	3	4	5	6
Laitila	ψ_{iL} (°)	302.53	293.97	291.65	287.73	286.92	286.78
(60.87 N, 21.60 E)	λ_{iL} (°)	22.12	19.80	17.03	14.92	12.47	10.47
Ruovesi	ψ_{iR} (°)	275.45	272.45	271.88	272.10	272.82	274.27
(61.82 N, 24.15 E)	λ_{iR} (°)	15.88	13.23	11.73	9.57	8.53	7.47

position of a great amount of known celestial objects at a given time and location on Earth. The dune equatorward tips were hence mapped to the local night sky with about 0.5° accuracy in azimuth ψ and elevation λ. The corresponding values are given in Table 1. The uncertainty to this method comes from two different aspects. First, the amount of stars visible in the pictures is limited, and hence some visual interpolation between some known stars had to be employed. Second, the dunes farther away at lower elevation angles are somewhat blurred because there are more emission targets between the observer and the dune location. However, those integrated effects do not prevent the unambiguous identification of each dune tip.

Let us consider the geocentric frame, in which O denotes the origin at the center of mass of the Earth. Let L represent Laitila and R represent Ruovesi, as denoted in Figure 3. Let (θ_L, φ_L) and (θ_R, φ_R) be the geographic latitude and longitude of Laitila and Ruovesi, respectively. For a given dune i, let P_i denote its equatorward tip, and let $(\lambda_{iL}, \psi_{iL})$ and $(\lambda_{iR}, \psi_{iR})$ be the elevation and azimuth of the dune tip when observed from Laitila and Ruovesi, respectively. Finally, let d_{iL} and d_{iR} be the distance between dune tip i and Laitila and dune tip i and Ruovesi, respectively.

We can write $\overrightarrow{OP_i} = \overrightarrow{OL} + \overrightarrow{LP_i} = \overrightarrow{OR} + \overrightarrow{RP_i}$. This can be written as a system of linear equations as follows:

$$\begin{cases} A_{x,iL}\, d_{iL} - A_{x,iR}\, d_{iR} = R_E \left(\cos\theta_R \cos\varphi_R - \cos\theta_L \cos\varphi_L \right) \\ A_{y,iL}\, d_{iL} - A_{y,iR}\, d_{iR} = R_E \left(\cos\theta_R \sin\varphi_R - \cos\theta_L \sin\varphi_L \right) \\ A_{z,iL}\, d_{iL} - A_{z,iR}\, d_{iR} = R_E \left(\sin\theta_R - \sin\theta_L \right), \end{cases} \quad (1)$$

with R_E the Earth radius and, bearing in mind that the azimuth is defined as positive eastward from the axis pointing toward the local north,

$$A_{x,iL} = -\cos\lambda_{iL} \cos\psi_{iL} \sin\theta_L \cos\varphi_L - \cos\lambda_{iL} \sin\psi_{iL} \sin\varphi_L + \sin\lambda_{iL} \cos\theta_L \cos\varphi_L$$

$$A_{y,iL} = -\cos\lambda_{iL} \cos\psi_{iL} \sin\theta_L \sin\varphi_L + \cos\lambda_{iL} \sin\psi_{iL} \cos\varphi_L + \sin\lambda_{iL} \cos\theta_L \sin\varphi_L$$

$$A_{z,iL} = \cos\lambda_{iL} \cos\psi_{iL} \cos\theta_L + \sin\lambda_{iL} \sin\theta_L$$
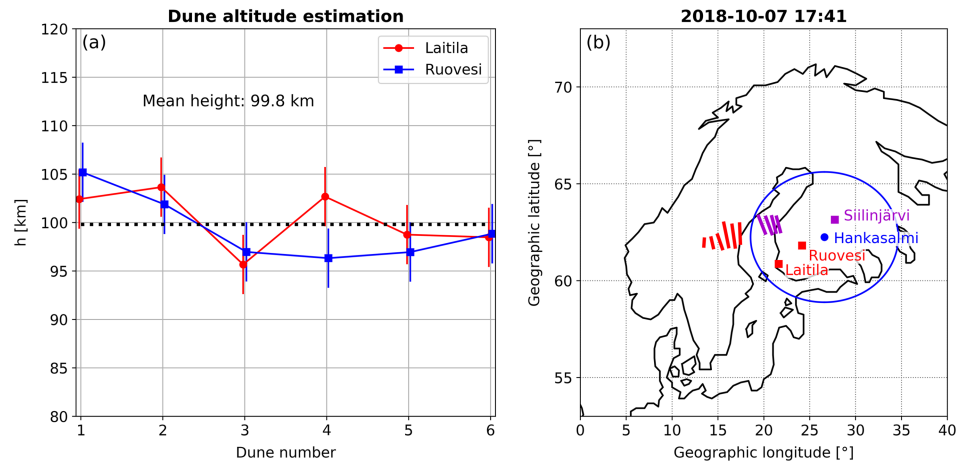

Figure 4. (a) Altitude of dunes numbered 1–6 (error bars from standard deviation). (b) Mapping of the dunes seen from Laitila and Ruovesi (red bars, taken simultaneously at 17:41 UT, see Figure 1). The Siilinjärvi dunes (see Figure 2a) are observed at 17:34 UT (purple). The Hankasalmi Observatory all-sky-camera field of view projected at 100 km altitude is given in blue.

and, similarly,

$$A_{x,iR} = -\cos\lambda_{iR}\cos\psi_{iR}\sin\theta_R\cos\varphi_R - \cos\lambda_{iR}\sin\psi_{iR}\sin\varphi_R + \sin\lambda_{iR}\cos\theta_R\cos\varphi_R$$

$$A_{y,iR} = -\cos\lambda_{iR}\cos\psi_{iR}\sin\theta_R\sin\varphi_R + \cos\lambda_{iR}\sin\psi_{iR}\cos\varphi_R + \sin\lambda_{iR}\cos\theta_R\sin\varphi_R$$

$$A_{z,iR} = \cos\lambda_{iR}\cos\psi_{iR}\cos\theta_R + \sin\lambda_{iR}\sin\theta_R.$$

For each dune i, the least squares solution of this system can be found for d_{iL} and d_{iR}, which yields two estimated positions for the dune tip P_i in the geocentric frame, $\overrightarrow{OP_{iL}}$ and $\overrightarrow{OP_{iR}}$. By calculating the norm of $\overrightarrow{OP_{iL}}$ and $\overrightarrow{OP_{iR}}$ and subtracting the local value of the Earth radius ($R_E \approx 6,359.5$ km at 61° latitude), we obtain two estimations of the altitude of P_i, h_{iL}, and h_{iR}, which are the values shown in Figure 4a in red and blue, respectively. The error bars given in Figure 4a correspond to the standard deviation of the two sets of six altitude estimates derived with this method.

2.2. Mapping to Ground and Wavelength Estimation

The solution to equation system (1) also gives the ground projection of the equatorward tips of the dunes. Since it proves more difficult to unambiguously identify the poleward ends of the dunes in both the Laitila and the Ruovesi pictures, their mapping to the ground is achieved using only one picture and assuming the altitude to be $h = 100$ km, that is, the altitude of the dunes as shown in Figure 4a. We used the Laitila picture for this purpose and the coordinates of vector $\overrightarrow{OP_{i'}} = \overrightarrow{OL} + \overrightarrow{LP_{i'}}$ in the geocentric frame, for each i' between 1 and 6, write

$$\begin{cases} OP_{i',x} = R_E\cos\theta_L\cos\varphi_L + \alpha A_{x,i'L} \\ OP_{i',y} = R_E\cos\theta_L\sin\varphi_L + \alpha A_{y,i'L} \\ OP_{i',z} = R_E\sin\theta_L + \alpha A_{z,i'L}, \end{cases} \tag{2}$$

where α is the unknown parameter to determine and $A_{x,i'L}$, $A_{y,i'L}$, $A_{z,i'L}$ completely analogous to $A_{x,iL}$, $A_{y,iL}$, $A_{z,iL}$, respectively, but for the poleward tips of the dunes instead of the equatorward tips. Since the altitude of the dunes is assumed, the equation to solve is

$$\|\overrightarrow{OP_{i'}}\|^2 = (R_E + h)^2, \tag{3}$$

which is a quadratic equation of unknown α:

$$\left(A_{x,i'L}^2 + A_{y,i'L}^2 + A_{z,i'L}^2\right)\alpha^2 + 2R_E\left(\cos\theta_L\cos\varphi_L A_{x,i'L} + \cos\theta_L\sin\varphi_L A_{y,i'L} + \sin\theta_L A_{z,i'L}\right)\alpha$$
$$- h\left(2R_E + h\right) = 0 \tag{4}$$

Once α is determined, the latitude and longitude of the considered dune tip are easily obtained by transforming the Cartesian coordinates of $\overrightarrow{OP_{i'}}$ to the spherical system. By applying a similar method for the poleward and equatorward ends of selected dunes in the Siilinjärvi picture taken at 17:34 (Figure 2a), one can then obtain the mapping of these dunes, as shown in Figure 4b. The wavelength of the dunes can then be estimated by dividing the distance from the tip of dune 1 to that of dune 6 by 5, that is, the number of intervals between dunes, which gives a value of 45 km. The error on this value can be evaluated by taking the standard deviation of the distances between two consecutive dunes, that is, 1–2, 2–3, …, 5–6, which gives 14 km. Hence, based on those calculations, the dunes observed during this event have a wavelength of 45 ± 14 km.

3. Dune Characteristics

From the method described in section 2.1, we estimated the altitude of the dunes to be around 100 km, as presented in Figure 4a, showing the dune fingertip altitudes in Laitila and Ruovesi with red and blue, respectively. Figure 4a shows that the dune fingers numbered with 1–6 all appear within a similar altitude range, indicating that the dunes appear within a layer of constant altitude of about 100 km. Since the triangulation method is based on identifying the same feature in simultaneous images, we verified the correct identification of the altitude by shifting the dune numbers in the Laitila image by +1 or −1 with respect to the numbers on the Ruovesi photograph and performed the altitude calculation with the shifted numbers. This test gives strong confidence in the altitude calculation, as it results in a slope in the altitude as a function of dune number, and the error bars are 4–6 times larger. This test essentially characterizes minimization of the error and indicates that the same dunes were indeed examined from both locations.
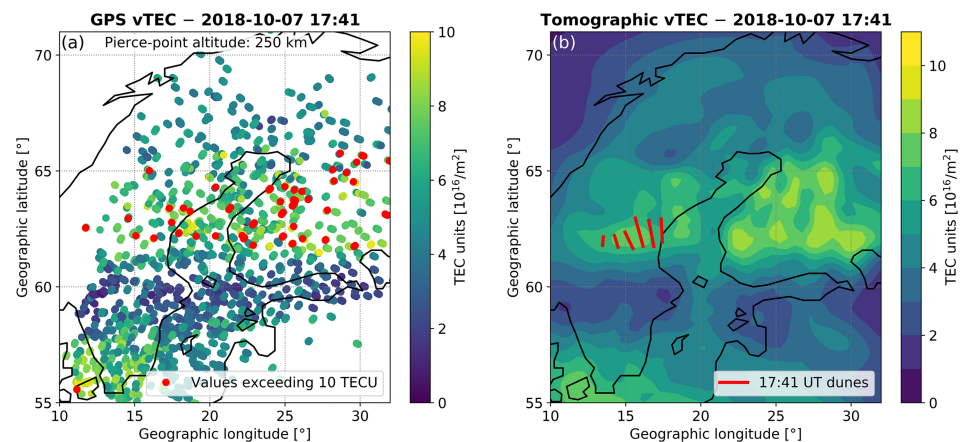
Figure 5. (a) Vertical total electron content (vTEC) using multiple simultaneous GPS satellite signals through the ionosphere at 17:37–17:41 UT and (b) ionospheric vertical TEC integrated from a three-dimensional GPS satellite tomography electron density reconstruction using data accumulated during 4 min. The dunes observed at 17:41 UT from Figure 4b are shown as red bars in panel (b).

Section 2.2 shows how the dune altitude can be used as a reference to determine their mapping to the ground. Based on section 2.2, the wavelength of the dune wave field is 45 ± 14 km. Figure 4b shows the mapping of the Laitila dunes to the ground by red color. By applying the same method for the poleward and equatorward ends of selected dunes in the Siilinjärvi picture taken at 17:34 (Figure 2a), one can then obtain the mapping of these dunes, as also shown in Figure 4b. The mapping procedure indicates that the dune wave field extends at least from 13°E to 22°E in geographic longitude, that is, from western Sweden to western Finland, and remains monochromatic across its entire extent. The pictures of the dunes show that the furthest waves are clearest, indicating stronger emission with a more slanted viewing angle, but no apparent wave structure near the zenith. In particular, in Ruovesi the dunes are not seen directly above (Figure 1b), even though the Ruovesi image zenith is near the mapped dune field from Siilinjärvi located further northeast. This suggests that the green emission comes from a thin layer, which can be seen when there are more emission targets along the line of sight.

The oscillation within the auroral emission is either due to the variation in the precipitating electron source or by undulations of the underlying atmospheric Oxygen density. To investigate this, Figure 5a presents ionospheric vertical total electron content (vTEC) at 17:37–17:41 UT at pierce points, at which the Global Positioning Satellite (GPS) radio signals intersect with a thin layer ionospheric model assumed to be at 250 km altitude, while Figure 5b presents ionospheric vTEC integrated from a three-dimensional GPS satellite tomography electron density reconstruction (Norberg et al., 2018). Essentially, Figure 5a is more directly based on actual measurements, but makes a more drastic assumption on the ionosphere and its height, which are more elaborately handled in Figure 5b. Figures 5a and 5b both show excess of electrons within the locations where the dunes were observed with digital cameras. Despite the zonal variation present in Figure 5, the zonal difference in the electron density is not significant within the tomographic accuracy (Norberg et al., 2018), suggesting that the resolution is not good enough to discern any longitudinal structures in the 45 km scale. To conclude whether there is a variation within the precipitation source, one needs spacecraft measurements above the dunes, which are not available during this event. However, the time lapse from the event (Movie S1) indicates that the dune rays seem rather stationary and appear and disappear as dictated by the stronger and weaker auroral emission. This gives the impression that the undulation is within the atmosphere, and that it is only illuminated by the aurora.

Another available subauroral data source is ground-based magnetometers, which are used to infer ionospheric equivalent currents (Amm & Viljanen, 1999) at 17:41 UT in Figure 6a. The dunes appear well in the center of the IMAGE magnetometer network, indicating that the estimated equivalent currents are representative; that is, the shape of the vector field is not distorted by currents outside of the measurement area. Figure 6a shows that the dunes are spatially colocated with a strong eastward horizontal electrojet. At (65°N, 23°E), the equivalent currents rotate anticlockwise, which is a strong sign of an upward field-aligned current (FAC), indicative of electron precipitation. The location is consistent with the discrete bright arc,
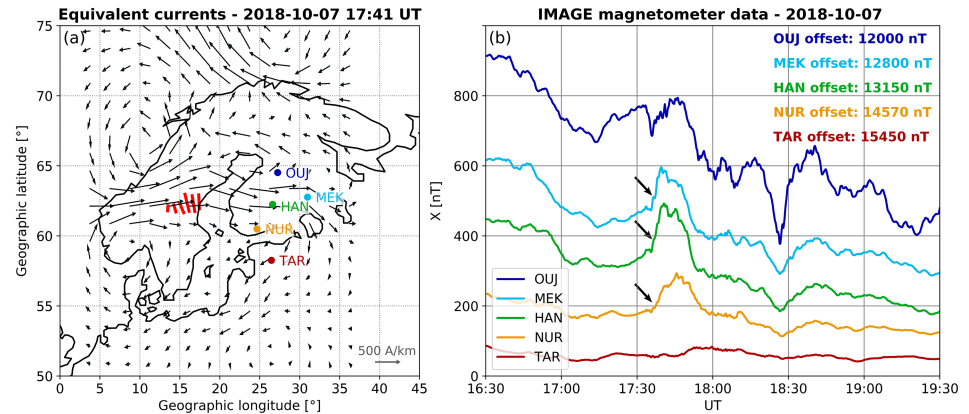
Figure 6. (a) Equivalent currents within the ionosphere at 17:41 UT, 7 October 2018. The dunes observed at 17:41 UT from Figure 4b are also shown as red bars. (b) Temporal evolution of the northward geomagnetic field component (X), which indicates eastward horizontal electrojets above the stations. The offsets, given at the top right corner of the panel, were defined such that the curves are ordered vertically according to the geomagnetic latitude of the corresponding magnetometer station. The black arrows indicate that the enhanced eastward electrojet was observed between stations MEK to NUR (see locations in panel b) roughly between 17:35 and 17:55 UT. The geomagnetic latitude range of stations TAR to OUJ is about 54.5° to 61°, respectively.

which is located just at the edge of the field of view of the all-sky-camera (Figures 2b and 4b). West from the Tartu (TAR) station, the equivalent currents suggest a downward current, indicating upwelling electrons. The location is consistent with the void of electrons within 58–60° latitude in Figures 5a and 5b. This current and electron density pattern is consistent with Region 1 and Region 2 FACs, which is common in the evening sector (Juusola et al., 2014). Figure 6b shows the temporal evolution of the northward component of the ground-level geomagnetic field, indicating that the eastward current is also temporally concurrent with the dunes.

The TEC and equivalent current observations can be used together to deduce the conditions for the dunes. The TEC observations (Figure 5) respond to variations of the ionospheric F layer, while the equivalent currents (Figure 6) in turn concern the electric currents in the E layer below. The enhancement of both at the same latitude range where the dunes appear would imply a broad energy spectrum in the auroral particle precipitation in that area, which would indicate auroral emission in a wide altitude range. As the dunes appear in contrast in a thin layer, we can conclude that their appearance in altitude is controlled rather by variations in the thermospheric oxygen content than by processes controlling auroral precipitation. Although not conclusive, this further suggests that the dunes are due to atmospheric undulation.

Table 2
*List of the Dune Events Caught by the Citizen Scientists Either Through the Open Taivaanvahti (*https://www.taivaanvahti.fi*) Service or Through Social Media Searches*

Day	Time	AE (nT)	SYM-H (nT)	Place
10 Oct 2018	17:36–17:45 UT	~550[*]	−42.5	Maaninka [63.2°N, 27.2°E]
7 Oct 2018	17:34–17:59 UT	~650[*]	−38.8	Several throughout Finland and Sweden
24 Oct 2017	~16:30 UT	756.5	−23.4	Sievi [63.9°N, 24.5°E]
13 Oct 2017	~17:00 UT	637.1	−49.5	Laitila
20 Jan 2016	17:00–17:30 UT	606.8	−86.1	Several places in Finland, Norway, Scotland
12 Oct 2015	~18:00–19:00 UT	687.2	−34.4	Several places throughout Southern Finland
7 Oct 2015	17:28–18:58 UT	1,166.9	−86.3	Several places throughout Southern Finland

Note. In the Taivaanvahti service the events can be accessed with this link (https://www.taivaanvahti.fi/observations/browse/pics/3210756). For all events, the available geophysical data are consistent with the behavior described in this paper. The AE and SYM-H columns give the average value of the AE and SYM-H indices, respectively, around the time of the observation, illustrating the geomagnetic activity conditions. The numbers marked with ([*]) are visually averaged from provisional data from the Kyoto Data Center for Geomagnetism (http://wdc.kugi.kyoto-u.ac.jp/index.html).

The solar wind data (not shown) during the event, retrieved from the OMNI data base (King & Papitashvili, 2005), indicate that the interplanetary magnetic field z component during the event is moderately negative around −3 nT, while the y and x components show an away-type Parker spiral conditions, indicating duskward interplanetary magnetic field with negative x. The solar wind speed is moderately increased and is slightly above 500 km/s. The solar wind conditions for the event are consistent with a high-speed stream coming from a coronal hole.

While we have presented geophysical data for 7 October 2018 in this article, the thorough investigation of the dune phenomenon yielded other events, shown in Table 2, which can be accessed in the open Taivaanvahti observation service maintained by the Finnish Association for Amateur Astronomers (Ursa). Table 2 gives the time and place of the dune observations as accurately as possible along with the geomagnetic conditions during the events. Since this 7 October 2018, event is the only event with coordinated campaign observations carried out in real-time guidance by scientists, the duration of the events is not known in all cases. The first clear event discussed among the citizen scientists is 7 October 2015. The observers report that the dunes are a rare phenomenon, faintly visible to the naked eye. Common to all reported events is the appearance of a monochromatic and horizontal wave field in the diffuse green aurora equatorward of the discrete arc. All events are recorded in the evening hours and are associated with a similar pair of upward and downward FACs as in Figure 6. All occur during moderate magnetic activity with AE (Davis & Sugiura, 1966) and SYM-H (Iyemori, 1990) indices ranging from 500 to 1,000 nT and −20 to −90 nT, respectively, during which the eveningside auroral zone is broader compared to nonactive times (Newell et al., 2009). All but one event are observed in October.

4. Interpretation and Conclusions

We have presented a new auroral form consisting of regular wave forms we call *the dunes*, which to our knowledge have not been reported before in scientific literature. We also developed a novel method to analyze citizen scientist photographs with which we can place the dunes into a thin layer that has a constant altitude of 100 km. The mapping of the dune field shows that the extent of the monochromatic waves spans at least from Sweden to Finland, with a wavelength of 45 km. Based on the supporting information Movie S1 and other supporting data we associate the dunes to the oscillation of the oxygen density, giving a variability to the auroral emission from the variability of the excitation targets within the atmosphere. While the evidence is not sufficient for us to conclude beyond a doubt that the dunes are not a manifestation of variations in the auroral precipitation, we argue they are more suggestive of them being a result of atmospheric waves.

The association of the dunes to the enhanced electron density and a pair of FACs may indicate at least two scenarios: First, the current system and enhanced electron densities simply indicate where the auroral zone is, suggesting that this is where the aurora acts like a torch illuminating the waves. Second, this kind of electrodynamic system including FAC and enhanced electron densities is associated with strong energy deposition from the magnetosphere, in the form of Joule heating (Palmroth et al., 2005) and electron precipitation (Palmroth et al., 2006). This may contribute to the phenomenon as we discuss below.

The first idea coming to mind to interpret the oscillation is based on atmospheric gravity waves, which are common at the dune altitudes (Rauthe et al., 2008). The north-south direction of the wave fronts would suggest a source at the Scandinavian mountains. However, mountain waves can be disturbed several times while propagating upward (Vadas, 2007; Xu et al., 2007), implying that the resulting wave field would not likely be horizontal nor monochromatic and would not extend over large distances without observable changes in the wave morphology. Further, as the diffuse aurora is rather common equatorward of the discrete arc (Sotirelis & Newell, 2000), one should see the dunes more often if they were "only" the common gravity waves illuminated by the common diffuse green emission. Therefore, we conclude that the dunes are not explained by "just" gravity waves. Indeed, the rarity of the events suggests that multiple trigger conditions may have to take place simultaneously to observe the dunes.

The monochromatic nature of the wave field suggests that spectral wave filtering may have occurred when the wave has propagated toward the 100 km altitude. Gravity wave filtering depends on mean zonal wind direction and speed in the stratosphere and mesosphere (Lukianova et al., 2015; Siskind et al., 2003; Xu et al., 2007). During the transition period between strong westward (summer) and eastward (winter) winds, for example, in October (Lukianova et al., 2018), the seasonally varying lower atmospheric winds could help to create suitable spectral filtering conditions for the gravity waves propagating upward. Such a scenario

has been suggested by Meriwether and Gerrard (2004). Even during wave filtering conditions, the spectrally filtered gravity waves would have to be ducted so that they could be observed as a horizontal wave field.

A possible cause for the dunes is a reportedly rare phenomenon called "mesospheric bore" (Miller et al., 2015) related to thin mesospheric inversion layers below the mesopause, associated to either increased temperatures or strong wind shears. The mesospheric inversion layer acts as a waveguide ducting gravity waves and allowing them to propagate horizontally and quasi-monochromatically over large distances without attenuation (Meriwether & Gerrard, 2004). The mesospheric bores are mostly observed in the low and midlatitudes (Su et al., 2018), very rarely near the poles (Nielsen et al., 2006), and to our knowledge never at the auroral zone using auroral emission for detecting them. This is because usually their detection is based on airglow and nightglow observations, which can be contaminated by the auroral emission (Su et al., 2018), leading to discard auroral latitudes in the majority of mesospheric bore studies. The morphology of the dune wave field is in good agreement with the mesospheric bores: the dunes exist within a thin layer, and the wave field has a large extent ranging from Sweden to Finland. The monochromatic wavelength of 45 km is consistent with mesospheric bores. Further, the mesospheric bore occurrence rate is largest around equinoxes (Su et al., 2018) and during evening hours (Hozumi et al., 2019).

Our results may open a new way of investigating the MLTI at subauroral latitudes, which are in general difficult to measure. There are only a few direct in situ spacecraft measurements due to the large neutral drag. Many instruments are either located further poleward at auroral zones (Röttger, 1994; Shiokawa et al., 2012), or the altitudes at which the instruments measure do not reach auroral altitudes. For example, gravity wave measurements using airglow instruments, lidars, and riometers can only be made up to about 90 km (Ehard et al., 2014; Jarvis et al., 2003; Shiokawa et al., 1999; Smith et al., 2000). Meteor radars can measure at around 100 km altitude (Su et al., 2014), but there are a limited number of such instruments at the dune latitudes. In general, gravity waves are not to our knowledge measured through auroral emission. The lack of direct observations of the MLTI at subauroral latitudes could be complemented by the large number of citizen observers there. Hence, the mesospheric bores could be observed more often if their detection is extended to include auroral emission.

The dunes may provide new insights into the structure of the mesopause as a response to driving by ionospheric energy deposition. Since all dune events occur during moderate magnetic activity (see Table 2) and are spatially and temporally associated with a FAC pattern that suggests energy deposition, it is intriguing to contemplate that the extra ionospheric energy deposition could contribute to the conditions favoring mesospheric bores. As stated above, the mesospheric bores require a ducting layer that according to a hydraulic jump theory (Dewan & Picard, 1998) can be formed either due to a layer of increased temperature below the mesopause, or by a wind shear above the mesopause. The ionospheric energy deposition could then contribute to the ducting layer by two mechanisms: First, if the mesopause is lifted to higher altitude than the layer at which the energy deposition from electron precipitation occurs, the additional precipitation energy might create or contribute to the mesospheric inversion layer by the additional energy through the heating of neutrals below the mesopause. This would be more likely with monoenergetic precipitation, during which the precipitation energy increases atmospheric temperature within a thin layer. Second, Joule heating deposits energy mainly at around 125 km altitude in the form of temperature that enhances neutral winds (Lu et al., 2016). Additional Joule heating could therefore strengthen the wind shear, which together with the mesopause below could act as a waveguide. To our knowledge neither mechanism has been suggested before, possibly due to the simple reason that mesospheric bores have not observed at auroral zones before. However, we emphasize that both the temperature enhancement and large wind shears required to create the waveguide could rather simply be provided by magnetospheric and ionospheric energy input, and to study this further one would need more dune observations at the auroral zones.

Finally, it is clear that the citizen scientist photographs are becoming accurate enough for scientific investigations (Archer et al., 2019). Due to the narrow field of view and good resolution, the new digital camera pictures can capture small-scale auroral features that can be difficult to discern in the more typical instrumentation. Further, as the majority of the citizens with cameras populate subauroral latitudes, the pictures are especially capturing subauroral physics, where ionospheric instrumentation placed at auroral latitudes are of limited use. Hence, we speculate that there will be an increasing number of studies with citizen scientists in the future, especially identifying new small-scale optical structures at subauroral latitudes.

Data Availability Statement

GPS TEC data products and access through the Madrigal distributed data system are provided to the community (http://www.openmadrigal.org) by the Massachusetts Institute of Technology (MIT) under support from US National Science Foundation Grant AGS-1242204. Data for TEC processing are provided from the following organizations: UNAVCO, Scripps Orbit and Permanent Array Center, Institut Geographique National, France, International GNSS Service, The Crustal Dynamics Data Information System (CDDIS), National Geodetic Survey, Instituto Brasileiro de Geografia e Estatística, RAMSAC CORS of Instituto Geográfico Nacional de la República Argentina, Arecibo Observatory, Low-Latitude Ionospheric Sensor Network (LISN), Topcon Positioning Systems, Inc., Canadian High Arctic Ionospheric Network, Centro di Ricerche Sismologiche, Système d'Observation du Niveau des Eaux Littorales (SONEL), RENAG: REseau NAtional GPS permanent, GeoNet—The official source of geological hazard information for New Zealand, GNSS Reference Networks, Finnish Meteorological Institute, and SWEPOS-Sweden. Access to these data is provided by madrigal network via this site (http://cedar.openmadrigal.org/). The IMAGE data are available online (https://space.fmi.fi/image/). We thank the institutes who maintain the IMAGE Magnetometer Array: Tromsø Geophysical Observatory of UiT the Arctic University of Norway (Norway), Finnish Meteorological Institute (Finland), Institute of Geophysics Polish Academy of Sciences (Poland), GFZ German Research Centre for Geosciences (Germany), Geological Survey of Sweden (Sweden), Swedish Institute of Space Physics (Sweden), Sodankylä Geophysical Observatory of the University of Oulu (Finland), and Polar Geophysical Institute (Russia). The solar wind data and the geomagnetic indices were retrieved from OMNIweb (https://omniweb.gsfc.nasa.gov), as well as World Data Center for Geomagnetism, Kyoto (http://wdc.kugi.kyoto-u.ac.jp/index.html).

References

Aikio, A. T., Cai, L., & Nygrén, T. (2012). Statistical distribution of height-integrated energy exchange rates in the ionosphere. *Journal of Geophysical Research*, *117*, A10325. https://doi.org/10.1029/2012JA018078

Amm, O., & Viljanen, A. (1999). Ionospheric disturbance magnetic field continuation from the ground to the ionosphere using spherical elementary current systems. *Earth, Planets and Space*, *51*(6), 431–440. https://doi.org/10.1186/BF03352247

Anderson, P. C., Heelis, R. A., & Hanson, W. B. (1991). The ionospheric signatures of rapid subauroral ion drifts. *Journal of Geophysical Research*, *96*(A4), 5785–5792. https://doi.org/10.1029/90JA02651

Andersson, M., Verronen, P., Rodger, C. J., Clilverd, M., & Seppälä, A. (2014). Missing driver in the Sun–Earth connection from energetic electron precipitation impacts mesospheric ozone. *Nature Communications*, *5*, 5197. https://doi.org/10.1038/ncomms6197

Archer, W. E., St.-Maurice, J.-P., Gallardo-Lacourt, B., Perry, G. W., Cully, C. M., Donovan, E., et al. (2019). The vertical distribution of the optical emissions of a Steve and Picket Fence event. *Geophysical Research Letters*, *46*, 10,719–10,725. https://doi.org/10.1029/2019GL084473

Arnold, N. F., & Robinson, T. R. (2001). Solar magnetic flux influences on the dynamics of the winter middle atmosphere. *Geophysical Research Letters*, *28*(12), 2381–2384. https://doi.org/10.1029/2000GL012825

Chereau, F. (2019). Stellarium. Github repository. Retrieved from https://github.com/Stellarium/stellarium (Version 0.19.1, last access: 06.11.2019).

Davis, T. N., & Sugiura, M. (1966). Auroral electrojet activity index AE and its universal time variations. *Journal of Geophysical Research*, *71*, 785–801. https://doi.org/10.1029/JZ071i003p00785

Dewan, E. M., & Picard, R. H. (1998). Mesospheric bores. *Journal of Geophysical Research*, *103*(D6), 6295–6305. https://doi.org/10.1029/97JD02498

Ehard, B., Achtert, P., & Gumbel, J. (2014). Long-term lidar observations of wintertime gravity wave activity over northern Sweden. *Annales Geophysicae*, *32*, 1395–1405. https://doi.org/10.5194/angeo-32-1395-2014

Gallardo-Lacourt, B., Liang, J., Nishimura, Y., & Donovan, E. (2018). On the origin of STEVE: Particle precipitation or ionospheric skyglow? *Geophysical Research Letters*, *45*, 7968–7973. https://doi.org/10.1029/2018GL078509

Hozumi, Y., Saito, A., Sakanoi, T., Yamazaki, A., Hosokawa, K., & Nakamura, T. (2019). Geographical and seasonal variability of mesospheric bores observed from the International Space Station. *Journal of Geophysical Research: Space Physics*, *124*, 3775–3785. https://doi.org/10.1029/2019JA026635

Iyemori, T. (1990). Storm-time magnetospheric currents inferred from mid-latitude geomagnetic field variations. *Journal of Geomagnetism and Geoelectricity*, *42*, 1249–1265.

Jarvis, M. J., Hibbins, R. E., Taylor, M. J., & Rosenberg, T. J. (2003). Utilizing riometry to observe gravity waves in the sunlit mesosphere. *Geophysical Research Letters*, *30*(19), 1979. https://doi.org/10.1029/2003GL017885

Juusola, L., Milan, S., Lester, M., Grocott, A., & Imber, S. (2014). Interplanetary magnetic field control of the ionospheric field-aligned current and convection distributions. *Journal of Geophysical Research: Space Physics*, *119*, 3130–3149. https://doi.org/10.1002/2013JA019455

King, J. H., & Papitashvili, N. E. (2005). Solar wind spatial scales in and comparisons of hourly Wind and ACE plasma and magnetic field data. *Journal of Geophysical Research: Space Physics*, *110*, A02104. https://doi.org/10.1029/2004JA010649

Lu, G. (2017). Large scale high-latitude ionospheric electrodynamic fields and currents. *Space Science Reviews*, *206*(1), 431–450. https://doi.org/10.1007/s11214-016-0269-9

Lu, G., Richmond, A. D., Lühr, H., & Paxton, L. (2016). High-latitude energy input and its impact on the thermosphere. *Journal of Geophysical Research: Space Physics*, *121*, 7108–7124. https://doi.org/10.1002/2015JA022294

Lukianova, R., Kozlovsky, A., & Lester, M. (2018). Climatology and inter-annual variability of the polar mesospheric winds inferred from meteor radar observations over Sodankylä (67N, 26E) during solar cycle 24. *Journal of Atmospheric and Solar-Terrestrial Physics*, *171*, 241–249. https://doi.org/10.1016/j.jastp.2017.06.005

Lukianova, R., Kozlovsky, A., Shalimov, S., Ulich, T., & Lester, M. (2015). Thermal and dynamical perturbations in the winter polar mesosphere-lower thermosphere region associated with sudden stratospheric warmings under conditions of low solar activity. *Journal of Geophysical Research: Space Physics*, *120*, 5226–5240. https://doi.org/10.1002/2015JA021269

MacDonald, E. A., Donovan, E., Nishimura, Y., Case, N. A., Gillies, D. M., Gallardo-Lacourt, B., et al. (2018). New science in plain sight: Citizen scientists lead to the discovery of optical structure in the upper atmosphere. *Science Advances*, *4*(3), eaaq0030. https://doi.org/10.1126/sciadv.aaq0030

Marchaudon, A., Blelly, P.-L., Grandin, M., Aikio, A., Kozlovsky, A., & Virtanen, I. (2018). IPIM modeling of the ionospheric F_2 layer depletion at high latitudes during a high-speed stream event. *Journal of Geophysical Research: Space Physics*, *123*, 7051–7066. https://doi.org/10.1029/2018JA025744

Meriwether, J. W., & Gerrard, A. J. (2004). Mesosphere inversion layers and stratosphere temperature enhancements. *Reviews of Geophysics*, *42*, RG3003. https://doi.org/10.1029/2003RG000133

Miller, S. D., Straka, W. C., Yue, J., Smith, S. M., Alexander, M. J., Hoffmann, L., et al. (2015). Upper atmospheric gravity wave details revealed in nightglow satellite imagery. *Proceedings of the National Academy of Sciences*, *112*(49), E6728–E6735. https://doi.org/10.1073/pnas.1508084112

Newell, P. T., Sotirelis, T., & Wing, S. (2009). Diffuse, monoenergetic, and broadband aurora: The global precipitation budget. *Journal of Geophysical Research*, *114*, A09207. https://doi.org/10.1029/2009JA014326

Nielsen, K., Taylor, M. J., Stockwell, R. G., & Jarvis, M. J. (2006). An unusual mesospheric bore event observed at high latitudes over Antarctica. *Geophysical Research Letters*, *33*, L07809. https://doi.org/10.1029/2005GL025649

Nishimura, Y., Gallardo-Lacourt, B., Zou, Y., Mishin, E., Knudsen, D. J., Donovan, E. F., et al. (2019). Magnetospheric signatures of STEVE: Implications for the magnetospheric energy source and interhemispheric conjugacy. *Geophysical Research Letters*, *46*, 5637–5644. https://doi.org/10.1029/2019GL082460

Norberg, J., Vierinen, J., Roininen, L., Orispaa, M., Kauristie, K., Rideout, W. C., et al. (2018). Gaussian Markov random field priors in ionospheric 3-D multi-instrument tomography. *IEEE Transactions on Geoscience and Remote Sensing*, *56*, 7009–7021. https://doi.org/10.1109/TGRS.2018.2847026

Palmroth, M., Hotakainen, M., & Jussila, J. (2018). *Revontulibongarin opas*. Helsinki, Finland: Into.

Palmroth, M., Janhunen, P., Germany, G., Lummerzheim, D., Liou, K., Baker, D. N., et al. (2006). Precipitation and total power consumption in the ionosphere: Global MHD simulation results compared with Polar and SNOE observations. *Annales Geophysicae*, *24*(3), 861–872. https://doi.org/10.5194/angeo-24-861-2006

Palmroth, M., Janhunen, P., Pulkkinen, T. I., Aksnes, A., Lu, G., Østgaard, N., et al. (2005). Assessment of ionospheric Joule heating by GUMICS-4 MHD simulation, AMIE, and satellite-based statistics: Towards a synthesis. *Annales Geophysicae*, *23*(6), 2051–2068. https://doi.org/10.5194/angeo-23-2051-2005

Röttger, J. (1994). Middle atmosphere and lower thermosphere processes at high latitudes studied with the EISCAT radars. *Journal of Atmospheric and Solar Terrestrial Physics*, *56*, 1173–1195. https://doi.org/10.1016/0021-9169(94)90056-6

Rauthe, M., Gerding, M., & Lübken, F.-J. (2008). Seasonal changes in gravity wave activity measured by lidars at mid-latitudes. *Atmospheric Chemistry and Physics*, *8*(22), 6775–6787. https://doi.org/10.5194/acp-8-6775-2008

Shiokawa, K., Katoh, Y., Satoh, M., Ejiri, M. K., Ogawa, T., Nakamura, T., et al. (1999). Development of optical mesosphere thermosphere imagers (OMTI). *Earth, Planets and Space*, *51*, 887–896. https://doi.org/10.1186/BF03353247

Shiokawa, K., Mori, M., Otsuka, Y., Oyama, S., & Nozawa, S. (2012). Motion of high-latitude nighttime medium-scale traveling ionospheric disturbances associated with auroral brightening. *Journal of Geophysical Research*, *117*, A10316. https://doi.org/10.1029/2012JA017928

Siskind, D. E., Eckermann, S. D., McCormack, J. P., Alexander, M. J., & Bacmeister, J. T. (2003). Hemispheric differences in the temperature of the summertime stratosphere and mesosphere. *Journal of Geophysical Research*, *108*(D2), 4051. https://doi.org/10.1029/2002JD002095

Smith, S. M., Mendillo, M., Baumgardner, J., & Clark, R. R. (2000). Mesospheric gravity wave imaging at a subauroral site: First results from Millstone Hill. *Journal of Geophysical Research*, *105*(A12), 27,119–27,130. https://doi.org/10.1029/1999JA000343

Sotirelis, T., & Newell, P. T. (2000). Boundary-oriented electron precipitation model. *Journal of Geophysical Research*, *105*(A8), 18,655–18,673. https://doi.org/10.1029/1999JA000269

Su, C. L., Chen, H. C., Chu, Y. H., Chung, M. Z., Kuong, R. M., Lin, T. H., et al. (2014). Meteor radar wind over Chung-Li (24.9°N, 121°E), Taiwan, for the period 10–25 November 2012 which includes Leonid meteor shower: Comparison with empirical model and satellite measurements. *Radio Science*, *49*(8), 597–615. https://doi.org/10.1002/2013RS005273

Su, Y., Yue, J., Liu, X., Miller, S. D., Straka, W. C., Smith, S. M., et al. (2018). Mesospheric bore observations using Suomi-NPP VIIRS DNB during 2013–2017. *Remote Sensing*, *10*, 1935. https://doi.org/10.3390/rs10121935

Vadas, S. L. (2007). Horizontal and vertical propagation and dissipation of gravity waves in the thermosphere from lower atmospheric and thermospheric sources. *Journal of Geophysical Research*, *112*, A06305. https://doi.org/10.1029/2006JA011845

Xu, J., Liu, H.-L., Yuan, W., Smith, A. K., Roble, R. G., Mertens, C. J., et al. (2007). Mesopause structure from Thermosphere, Ionosphere, Mesosphere, Energetics, and Dynamics (TIMED)/Sounding of the Atmosphere Using Broadband Emission Radiometry (SABER) observations. *Journal of Geophysical Research*, *112*, D09102. https://doi.org/10.1029/2006JD007711